Article

Plasmon-Enhanced Electrochemiluminescence of Silver Nanoclusters for microRNA Detection

Xiuyun Feng, Ting Han, Yunfang Xiong, Sicheng Wang, Tianyue Dai, Jihua Chen, Xiaojun Zhang, and Guangfeng Wang

ACS Sens., **Just Accepted Manuscript** • DOI: 10.1021/acssensors.9b00413 • Publication Date (Web): 05 Jun 2019

Plasmon-Enhanced Electrochemiluminescence of Silver Nanoclusters for microRNA Detection

Xiuyun Feng, Ting Han, Yunfang Xiong, Sicheng Wang, Tianyue Dai, Jihua Chen, Xiaojun Zhang, Guangfeng Wang*

Key Laboratory of Chem-Biosensing, Anhui province; Key Laboratory of Functional Molecular Solids, Anhui province; College of Chemistry and Materials Science, Center for Nano Science and Technology, Anhui Normal University, Wuhu 241000, PR China

ABSTRACT: Surface plasmon-enhanced electrochemiluminescence (SPEECL) with excellent sensitivity and simplicity has attracted increasing attention. In this work, we reported a novel SPEECL with DNA templated silver nanoclusters (DNA-AgNCs) as ECL emitters and gold nanoparticles (AuNPs) as localized surface plasmon resonance (LSPR) source. The SPEECL with DNA-AgNCs as ECL luminophores possessed low-toxicity and avoided the labelling process, which is favorable for its further sensing application. In addition, by investigation of the SPEECL under different distances between DNA-AgNCs and AuNPs, it was demonstrated the SPEECL was distance dependent. Meanwhile, the SPEECL intensity changed with the sizes and inter-distance of AuNPs under different electrodeposition time. Furthermore, by the combination of a cyclic amplification process with enzyme-free catalytic hairpin DNA, a sensitive SPEECL biosensor was proposed for the detection of microRNA (miRNA-21) successfully with a wide linear range from 1 aM to 10^4 fM and a relatively low detection limit of 0.96 aM, which was applied in the detection of miRNA-21 in real samples with satisfying results. This novel, simple, sensitive and selective SPEECL with label-free and low-toxic ECL emitters displayed a great potential for bioassay application.

KEYWORDS: surface plasmon-enhanced electrochemiluminescence, silver nanoclusters, gold nanoparticles, catalytic hairpin assembly, miRNA-21

Since the nineties of the 20th century, intensive studies on the domain of spectroscopy enhanced by plasmon are springing up vigorously accompanying with the development of material science and nanotechnology.[1-4] Specially, in localized surface plasmon resonance (LSPR), the free electron collectively oscillate in metal nanostructures inspired by the electromagnetic (EM) field, can induce remarkable enhancement of the optical signals such as fluorescence,[5-7]electrochemiluminescence (ECL),[8-12] Raman scattering,[13-15] or infrared absorption,[16] leading to a family of plasmon-enhanced spectroscopies. Because of its intriguing optical properties, this surface plasmon triggered photoluminescence enhancement has increasingly been applied in enormously multidisciplinary fields including biological analysis,[17-19] catalysis,[20] and material science.[9]

Especially, surface plasmon-enhanced electrochemiluminescence (SPEECL) with excellent sensitivity and simplicity has been developed in various chemical and biomedical assays, because electrodes were used as the energetic origin for emission, avoiding the requirement of being illuminated by an exterior light resource and favorable to assay with high throughput. Lakowicz and co-workers firstly observed the surface plasmon coupled ECL from $[Ru(bpy)_3]^{2+}$ on Au film electrode.[21,22] Later, Xu's group reported the enhanced ECL of CdS : Mn nanoparticels (NPs) induced by the excited surface plasmon resonances of AuNPs, which was fabricated for the detection of DNA sensitively. In addition, by comparison with resonance energy transfer (RET), they found the SPEECL was closely related with the distance between the surface plasmon source and ECL luminescent luminophores. [23] Very recently, surface plasmon from Au nanoparticles to enhance ECL intensity of Au nanoclusters (NCs) was also disclosed and applied for the ratiometric detection of miRNA.[24] Nevertheless, up to now, despite some SPEECL by the LSPR of noble metal nanostructures has been investigated, most luminophores in SPEECL are limited in Ru complex,[9,25] AuNCs,[24] quantum dots (QDs),[26-28] or other semiconductor nanocrystals, which is prone to suffer from the complex process of labelling, or the inherent toxicity, greatly restricting their bio-applications. Consequently, the exploration of novel label-free ECL species with low or no toxicity for SPEECL is extremely desirable.

Profiting from their particularly small size, AgNCs with dramatically different optical, electrical, and chemical properties.[29-31] have been proven to possess potential applications in chemical sensing, optical assay and biological imaging.[32-35] Since Ras et al. firstly discovered the ECL features of AgNCs in 2009,[36] AgNCs have drawn gradual interest as novel ECL luminophores. More recently, DNA-stabilized AgNCs, integrated the features of electrochemical generated luminescent of AgNCs and the biorecognition of flexible DNA, possessing various fascinating properties, eg. dispensable with labelling process, low-toxicity and extremely stability, have been extensively utilized as ECL luminophores in miscellaneous bioassays.[37]For instance, Yuan's group utilized AgNCs by in-situ electrogneration as ECL luminophores with a coreaction accelerator of

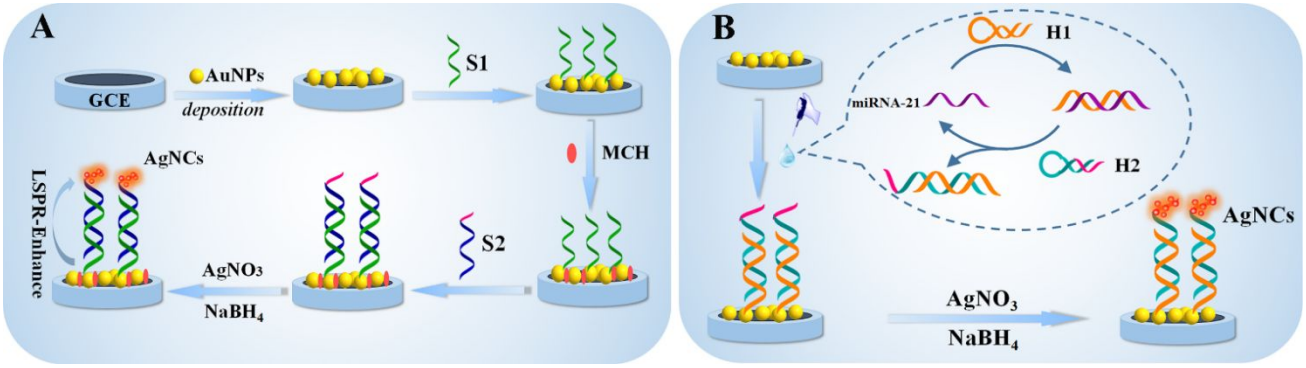

Scheme 1. (A) Schematic Illustration of the Structure and Modification Process of the Surface Plasmon-Enhanced ECL Electrode (B) Based on SPEECL Biosensor for miRNA-21 Detection.

Fe_3O_4–CeO_2 nanocomposites to fabricate Cyclin-D1 ECL biosensor with high sensitivity.[38] In addition, with intrinsic O_2 as the coreactant and AgNCs as ECL emitters, ultrasensitive ECL detection of amyloid-β was developed.[39] Furthermore, combining the ECL signals of AgNCs with signal amplification strategy of target-cycling and rolling circle amplification, an unltrasensitive ECL platform for miRNA detection was fabricated.[40] Specially, Zhang et al. found a decreased ECL intensity of AgNCs took place originated from the resonance energy transfer (RET), and further applied for the preparation of a quenched ECL sensor of miRNA.[41] However, to the best of our knowledge, there is no report on SPEECL emission of AgNCs and its further bioapplications.

Inspired by the above mentioned studies, in this paper, a novel SPEECL models containing DNA-templated AgNCs as ECL luminophores and AuNPs as surface plasmon resonance sources was reported, and further for highly sensitive detection of miRNA-21. It was found that the SPEECL was dependant on the separation distance between AgNCs and gold nanoparticles, which was exploited by conjugating with different lengths of DNA sequences. Moreover, the electrodeposition time of gold nanoparticles also had a vital effect on the ECL intensity of AgNCs. Finally, by the combination of catalytic hairpin assembly amplification (CHA), the SPEECL of AgNCs was applied to fabricate ultrasensitive biosensor in the detection of miRNA-21, which displays a potential prospect of bioanalytical application.

EXPERIMENTAL SECTION

The descriptions of "Materials and Reagents", "Apparatus" are described in the Supporting Information.

Electrochemical Deposition of AuNPs on the Glassy Carbon Electrode Surface. To deposit AuNPs on the glassy carbon electrode surface, the electrochemically cleaned GCE needs to be pretreated. First, the GCE was polished with gradually refined sand papers and further burnished to a mirror-like surface with alumina slurries (the mean diameters of Al_2O_3 particle is 0.3 and 0.05 μm) on polishing chamois leather. Then, the GCE was thoroughly rinsed with ultrapure water and ultrasonicated in ethanol and water by turns, followed by the drying of the cleaned electrode at room temperature. Finally, electrodeposition was performed at a fixed potential of -0.2 V in 0.01 wt% $HAuCl_4$ for different periods of time including 10, 15, 30, 40, or 60 seconds, respectively.

Fabrication of the Surface Enhanced ECL Electrode. Prior to modification, a AuNPs/GCE was obtained according to the above statements, and then 8 μL of S1 DNA with -SH modified (5 μM) was dipped onto the AuNPs/GCE at ambient temperature for 12 h to assemble S1 on the AuNPs/GCE (S1/AuNPs/GCE) by the covalent bond of Au–S. Furthermore, the S1/AuNPs/GCE was washed with washing buffer and blocked with 8 μL of 10 mM 2-mercaptoethanol (MCH) for 1 h at room temperature to prohibit nonspecific conjugation. After being washed thoroughly and dried in nitrogen, the S1/AuNPs/GCE modified electrodes were dropped with 8 μL DNA S2 (5 μM), which were partly complementary with S1 to fabricate S2-S1/AuNPs/GCE. Furthermore, 8 μL of 30 μM $AgNO_3$ solution was dipped onto the surface of S2-S1/AuNPs/GCE and incubated in dark for 30 min to prepare AgNCs followed by dipping 8 μL of 30 μM fresh $NaBH_4$ solution carefully onto the above electrode surface and incubating in dark at ambient temperature for 2 h. Finally, the obtained AgNCs on S2-S1/AuNPs/GCE electrodes were obtained (AgNCs/S2-S1/AuNPs/GCE) and washed with the washing buffer followed by drying for electrochemical and ECL measurements. In order to discuss the role of distance between the AuNPs and the AgNCs on ECL emission, different length dsDNA structures (S4-S3, S6-S5, S8-S7, S10-S9) instead of S2-S1 was assembled, and then the obtained modified electrode named as AgNCs/S4-S3 (S6-S5, S8-S7, or S10-S9)/AuNPs/GCE were washed with the washing buffer and dried for ECL measurements according to the above statements. Control electrode of AgNCs/S2-S1/GCE was prepared as the above steps except the deposition of AuNPs.

Fabrication of the miRNA Biosensor. The biosensor based on the target miRNA-21-triggered catalyzed hairpin assembly amplification was exploited by incubating a series of concentrations of target miRNA-21 into 16 μL Tris buffer containing 5 μM hairpin DNA (H1) and cytosine-rich hairpin (H2) at 37 °C for 2 h. Meanwhile, the cleaned glassy carbon electrode was modified with Au nanoparticles in optimized electrodeposition time, and then the AuNPs/GCE modified electrodes were incubated with the products (H1-H2 complexes, which were obtained through the target miRNA-21-triggered catalytic hairpin assembly amplification) at 37 °C for 2 h to obtain H2-H1/AuNPs/GCE following that the electrodes were washed with washing buffer and dried. Furthermore, the AgNCs were prepared on H2-H1/AuNPs/GCE as the above described on S2-S1/AuNPs/GCE to prepare AgNCs/H2-H1/AuNPs/GCE. Finally, the electrodes were washed with the washing buffer and dried for electrochemical and ECL measurements.

Gel Electrophoresis. 10 μL of the prepared sample was put on agarose gels (5%). The electrophoresis was carried out in 0.5 × TBE buffer with stationary potential of 120 V for 60 min. After EB staining, the gels were scanned using the Omega 16ic Gel imaging system (ULTRA-LUM, USA).

RESULTS AND DISCUSSION

Principle and Characterization of the SPEECL Electrode. In order to investigate the SPEECL with DNA-templated AgNCs as ECL luminophores and AuNPs as surface plasmon resonance enhanced sources, we designed the modified electrode as shown in Scheme 1A. First, AuNPs were modified on the surface of the GCE (AuNPs/GCE) by using electrochemical deposition. Subsequently, the single stranded substrate DNA probe S1 was conjugated onto the AuNPs/GCE by Au-S interaction and then the obtained electrode was blocked with MCH to seal the nonspecific active sites. Furthermore, by the complementary bases of S2 at 3' end with S1, a DNA duplex was formed on the electrode to prepare S2-S1/AuNPs/GCE. Because bases at the 5' end of S2 were designed with cytosine- rich sequence, after incubating the duplex modified electrode with $AgNO_3$ and the reduction of $NaBH_4$, DNA-templated AgNCs were formed on the duplex (AgNCs/S2-S1/AuNPs/GCE). The characterization of the formed DNA-AgNCs is shown in Figure S1A with the typical high resolution transmission electron microscopy (HRTEM) images. As we can be seen from the HRTEM image, the AgNCs with an average diameter about 3 nm were uniformly distributed in the field of view. Figure S1B-D showed the scanning electron microscopy (SEM) images and X-ray energy dispersive spectroscopy (EDS) of different electrodes. As shown in Figure S1B, compared with the obvious Au nanoparticles on GCE (Figure 4), a blurred film was observed after S1 and S2 were assembled on AuNPs/GCE, may be due to the weak electrical conductivity of DNA. As for the AgNCs/S2-S1/AuNPs/GCE, obviously larger AuNPs could be seen, maybe due to the existence of AgNCs enhanced the electrical conductivity. As shown in Figure S1D, the EDS characteristic peaks of Au and Ag indicated that the AgNCs/S2-S1/AuNPs/GCE was successfully fabricated.

To prove the stepwise assembled processes of the above modified electrode, the surface process of the electrodes was characterized by the cyclic voltammograms (CVs) and electrochemical impedance (EIS) spectra in the solution containing $[Fe(CN)_6]^{3-/4-}$ probes. As shown in Figure 1A, a well-defined redox peak of $[Fe(CN)_6]^{3-/4-}$ appeared on the bare GCE (curve a) and the same redox peak current on AuNPs/GCE increased obviously because the conductivity of AuNPs is favorable for the improvement of the electron transportation (curve b). With the immobilization of S1 and MCH in turns, the peak currents decreased gradually (curves c and d), which was due to that S1 and MCH blocked the contact of the redox probe with the electrode surface. When S2 was conjugated with S1, the duplex was assembled and further AgNCs were formed on the modified electrode. The redox currents decreased because the existence of the dsDNA on the electrode surface with more negative charges resulting in the electrostatic repulsive-force towards $[Fe(CN)_6]^{3-/4-}$ (curve e). It demonstrated that the modified electrode was successfully fabricated. The electrode modified steps were further characterized by electrochemical impedance spectra. The classical impedance spectrum contains a semicircular region at high frequencies whose diameter equals to the electron transportation resistance, Ret. As shown in Figure 1B, a small semicircle appeared on the bare GCE (curve a) and the Ret lowered on the AuNPs/GCE (curve b), implying the good conductivity of AuNPs. After the assembly of S1 and MCH, the electron transfer resistance increased (curves c and d) attributed to that the phosphoric acid backbone of oligonucleotides with negative charge inhibited the approaching of the same charged $[Fe(CN)_6]^{3/4-}$. After the duplex (S1-S2) formed on the modified electrode and the assembling of AgNCs (curve e), the Ret increased further, possibly due to that the duplex hindered the electron transfer, in accordance with the results from CVs.

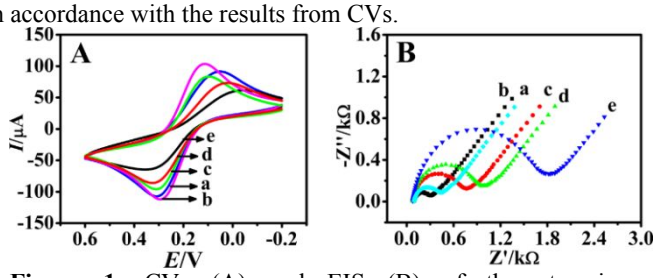

Figure 1. CVs (A) and EIS (B) of the stepwise modifications of electrodes tested in 5.0 mM $[Fe(CN)_6]^{3-/4-}$ containing 0.1 M KCl (scan rate: 100 mV/s). (a) bare GCE, (b) AuNPs/GCE, (c) S1/AuNPs/GCE, (d) MCH/S1/AuNPs/GCE, (e) AgNCs/S2-S1/AuNPs/GCE.

Mechanism of the proposed SPEECL. Furthermore, to investigate the ECL enhancement of AgNCs by AuNPs, ECL experiment with different modified electrodes in the PBS containing 0.05 M $K_2S_2O_8$ and 0.1 M KCl was carried out in the potential window of 0 to -1.6 V. Figure 2A showed that the background ECL on the bare GCE was small (curve a). As the the modification of AuNPs, the ECL signal improved (curve b). Furthermore, compared with the ECL response of AgNCs/S2-S1/GCE (curve c), the AgNCs/S2-S1/AuNPs/GCE (curve d) displayed enhanced ECL responses. In the course, the luminescent AgNCs and coreactant $S_2O_8^{2-}$ in the ECL system were first reduced to form $AgNCs^{-\bullet}$ and $SO_4^{-\bullet}$. And then, the $AgNCs^{-\bullet}$ could be oxidized by $SO_4^{-\bullet}$ to AgNCs*. It could emit the light from excited to ground state and consequently the ECL intensity could be obtained. The whole ECL process could be described as follows:

$$AgNCs + e^- \rightarrow AgNCs^{-\bullet} \quad (1)$$

$$S_2O_8^{2-} + e^- \rightarrow SO_4^{2-} + SO_4^{-\bullet} \quad (2)$$

$$AgNCs^{-\bullet} + SO_4^{-\bullet} \rightarrow AgNCs^* + SO_4^{2-} \quad (3)$$

$$AgNCs^* \rightarrow AgNCs + h\nu \quad (4)$$

However, as expected, the ECL intensity of AgNCs/S2-S1/AuNPs/GCE was much (about 8.5 times) higher than that of AgNCs/S2-S1/GCE. We suggest the enhanced ECL is originated from two possible sources. First, the "nanoelectrode'' effect may improve the ECL signal because the electrode modified with AuNPs may enlarge the surface area and load more DNA and further AgNCs. However, according to the CVs response of AgNCs/S2-S1/AuNPs/GCE and AgNCs/S2-S1/GCE (control electrode) in 0.1 M PBS solution containing 0.05 M $K_2S_2O_8$ and 0.1 M KCl, the electrodes with and without modification of AuNPs showed almost the same profile (Figure S2), implying the ECL signal enhancement by "nanoelectrode" effect could be ignored. In consequence, the LSPR of AuNPs should mostly attribute to the great enhancement of ECL. Furthermore, the emission spectrum of AgNCs and UV−vis absorption spectrum of AuNPs were examined to investigate whether the emission spectrum of the donor could rightly match the absorption spectrum of the acceptor to confirm the principle of LSPR

enhancement.[42]As Figure 2B displayed, the ECL emission peak of AgNCs was at 552 nm (curve b), well overlapped with the plasmon absorption band of AuNPs centered at 522 nm (curve a), implying a feasible LSPR-ECL couple. In general, the LSPR of AuNPs was first excited with the enhanced electromagnetic near-field which coupled back into the emission of AgNCs* resulting in the SPEECL.

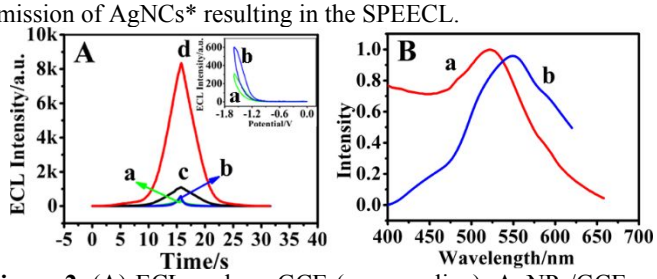

Figure 2. (A) ECL on bare GCE (a, green line), AuNPs/GCE (b, bule line), AgNCs/S2-S1/GCE (c, black line) and AgNCs/S2-S1/AuNPs/GCE (d, red line) in 0.1 M PBS (pH 7.4) containing with 0.05 M $K_2S_2O_8$ and 0.1 M KCl (Scan rate: 100 mV/s, inset: ECL intensity-potential curve of bare GCE and AuNPs/GCE). (B) UV-vis absorption spectrum of AuNPs (a, red line) and ECL emission spectrum of AgNCs (b, blue line).

Influence of Separation Distance Between AgNCs and AuNPs for SPEECL. Since the distance between the luminophores and surface plasmon resonance sources acts as a two-edged sword to the ECL emission as reported,[23] the optimization of the inter-distances between AgNCs and AuNPs to achieve optimal ECL enhancement was exploited. A series of duplex (S6-S5, S4-S3, S2-S1, S8-S7, S10-S9) containing various complementary bases pairs of 18, 27, 36, 45 and 54 bp with different lengths (1 nm for 3-base) was assembled on the AuNPs/GCE. Because of the –SH at 5' end of S1 (S3, S5, S7, or S9), they could be assembled on the AuNPs/GCE and formed the duplex on the electrode by the hybridization with their complementary strands (S2, S4, S6, S8, or S10). Since the complementary strands containing the cytosine- rich base at 5' end, it would result in different separation distances between the AgNCs on the end of the duplex and AuNPs on the surface of GCE. As shown in Figure 3, when the number of complementary bases was 18 bp, the ECL signal was weak (curve a). It suggested the close distance between the AgNCs and AuNPs may result in the generation of ECL resonance energy transfer (ECL-RET) processes from the AgNCs towards the Au nanoparticles to decrease ECL intensity. With the numbers of complementary bases increased to 27 and 36 bp, the ECL intensities were dramatically enhanced by 3.6-fold and 7.8-fold (curves b and c). As reported in experiment and theory, the distance between luminophores and AuNPs is key to the occurrence of ECL-RET and LSPR enhancement.[43,44] Because the ECL-RET usually appears in a short distance, and it decreased with the distance enlarged more seriously than the enhanced SPR field, the effect of LSPR is the main sources of the ECL enhancement and the ECL-RET could be ignored in this case. After further increasing the numbers of complementary bases to 45 and 54 bp, the enhanced efficiencies decreased to 5.2-fold and 2.8-fold (curves d and e). It was suggested that the SPR field are dumping exponentially with the increasing distance. Consequently, the ECL intensity decayed when the distance between AgNCs and AuNPs increased furthermore. Therefore, the maximum ECL intensity was observed when the complementary bases were 36 bp with about 12 nm of the separation distance. The above phenomenon confirmed the effect of inter-distance on the LSPR between AgNCs and AuNPs.

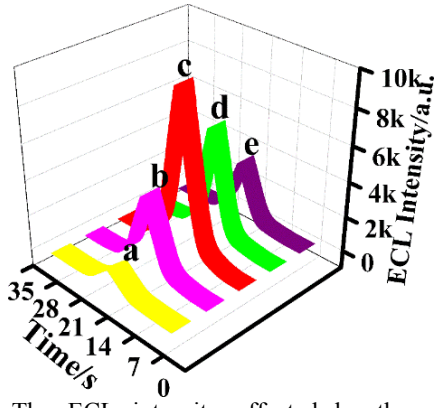

Figure 3. The ECL intensity affected by the separation distance between AgNCs and AuNPs through controlling numbers of base pairs in the duplex: 18 (a), 27 (b), 36 (c), 45 (d), and 54 (e) bp.

The Effect of Electrochemical Deposition Time of Gold Nanoparticles on SPEECL. Furthermore, the electrodeposition time of AuNPs on GCE on the intensity of SPEECL was investigated. A series of electrodepostion time from 10 to 60 seconds was used to deposit AuNPs on the cleaned GCE and then the assembly of AgNPs/S2-S1/AuNPs/GCE was fabricated with the same steps. The ECL of these AgNCs/S2-S1/AuNPs/GCE electrodes was investigated. The typical SEM images were shown in Figure 4A-E, it could find that the quasi-spherical AuNPs have been successfully immobilized on the electrode with a quite symmetric distribution. With the time increased from 10 to 30 seconds, the sizes of nanoparticles were found to be enlarged. For example, the average size of AuNPs is approximately 20 nm for an electrodeposition time of 10s (Figure 4A), while it is approximately 50 nm for 30 seconds (Figure 4C) under the same electrodeposition conditions. The average size of AuNPs increased from about 50 nm to 80 nm (Figure 4E) when the time of electrodeposition was increased from 30 to 60 seconds. We note that the increased size of AuNPs and the decreased inter-distance of AuNPs mostly depends on the elongation of electrodeposition time. In addition, with the inter-distance of AuNPs becoming smaller, the SPEECL was affected maybe due to the inhibited growth of gold nanoparticles.[45] Figure 4F showed the relationship between the corresponding SPEECL signals and electrodeposition time of AuNPs. When the electrodeposition time was 10 seconds, the ECL signal was slight (curve a). With the electrodeposition time increased to 15 seconds, the ECL intensities were significantly enhanced by 5.8-fold (curve b). Best ECL enhancement was observed with electrodeposition time of 30 seconds (curve c). However, continuously extending the deposition time, the ECL intensity decreased gradually. After further increasing the deposition time to 40 and 60 seconds, the enhanced efficiencies decreased to 3.1-fold and 1.7- fold (curves d and e). Thus, the electrodeposition time affecting the size and inter-distance of AuNPs has an obvious effect on the SPEECL.

Fabrication of AgNCs Based miRNA-21 SPEECL Biosensor. Based on the LSPR of AuNPs enhanced ECL emission of AgNCs, furthermore, a novel detection strategy with target-triggered enzyme-free catalytic hairpin assembly was developed for highly sensitive detection of miRNA-21. As shown in Scheme 1B, two DNA hairpins (H1 and H2) were

designed for the CHA reaction. In the presence of target miRNA-21, the hairpin DNA H1 with 5'-thiol modified is opened by hybridizing with target through complementary sequences. Then, by hybridization of H1 with another hairpin DNA H2 generating H1-H2 duplex

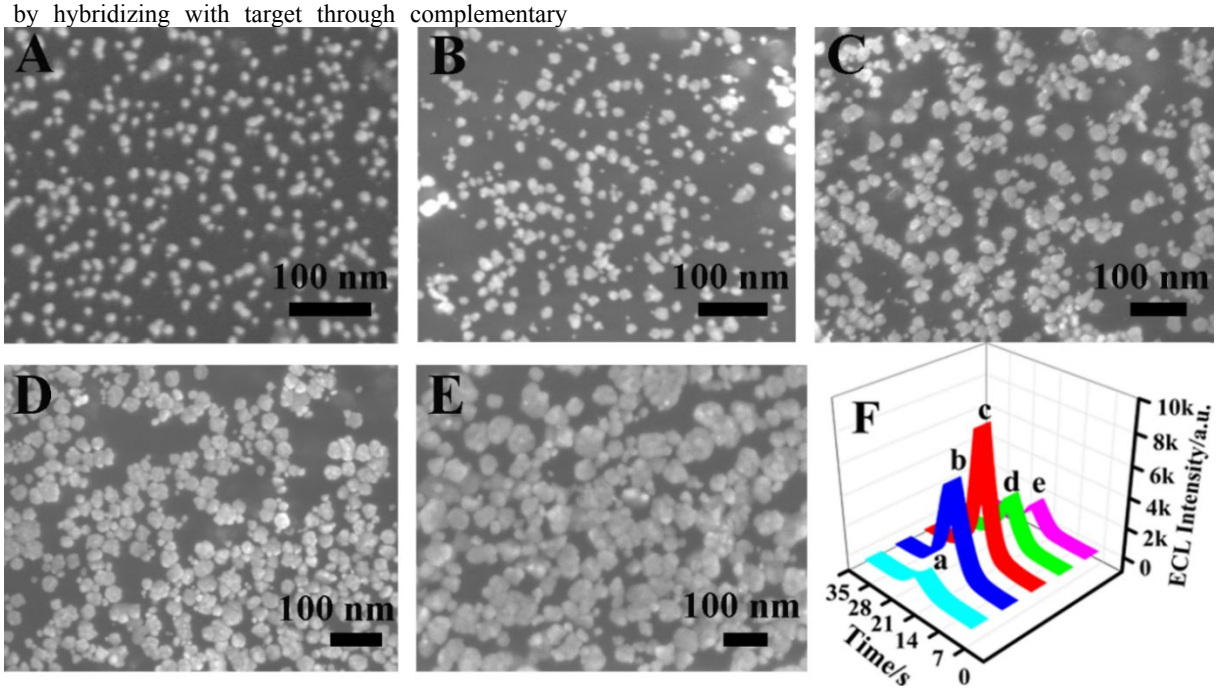

Figure 4. SEM images (A-E) and the corresponding ECL intensity (F) under different electrodeposition time of AuNPs: 10 (A, a), 15 (B, b), 30 (C, c), 40 (D, d) and 60 seconds (E, e)

complex, the target could be released from the H1-H2 duplex and initiated many cycles for the generation of large amounts of H1-H2 duplex contributing to signal amplification. After that, by the covalent bond of Au−S, these H1-H2 duplexes were assembled onto the AuNPs modified electrode. By the same reduction method as Scheme 1A described, a large amount of AgNCs were grown on the H1−H2 duplexes and achieved the strong electrochemiluminescence signals. The corresponding electrochemical characterization of the AgNCs based miRNA biosensor was shown in Figure S3.

Meanwhile, gel electrophoresis assays were carried out to demonstrate the amplification strategy of CHA. As show in Figure 5, distinctly single band from miRNA-21, H1, and H2 in lanes 1, 2, and 3 was observed, respectively. Lanes 4 and 5 were corresponding to the bands of_a mixture of H1/H2 and the hybridization of miRNA-21/H1/H2 template. Moreover, the H1/H2 mixture showed the original bands of H1 and H2 monomers, implying that if without the target, the CHA amplification was blocked. However, as with the target of miRNA-21, a slower electrophoretic mobility can be investigated (lane 5), demonstrated the feasibility of CHA strategy.

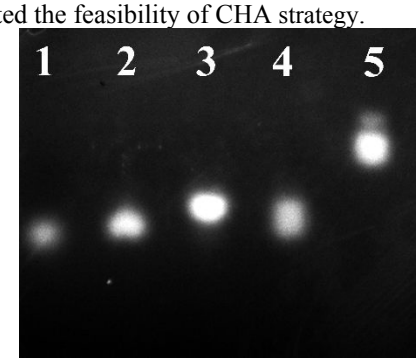

Figure 5. Gel electrophoresis assay: lane 1, miRNA-21; lane 2, H1; lane 3, H2; lane 4, mixture of H1 and H2; lane 5, mixture of H1, H2, and miRNA-21.

Assay Performance of AgNCs Based SPEECL Biosensor for miRNA-21 Detection. Under the optimal experimental conditions (Supporting Information), the assay performance of the present miRNA-21 SPEECL biosensor was investigated. As shown in Figure 6A, the ECL responses towards different concentrations of miRNA-21 were recorded. It was obvious that the ECL intensity enlarged with the increase of miRNA-21 concentrations (curves a–h). As shown in Figure 6B, ECL signal was linearly related with the logarithm of miRNA-21 concentrations in the range of 1 aM to 10^4 fM with a regression equation of I=4415.81+1041.15logc (I: ECL intensity, c: the concentration of miRNA-21) and a linear correlation coefficient of 0.9933. Additionally, an estimated detection limit of 0.96 aM (S/N=3) could be obtained. Compared with other miRNA-21 biosensors, the present SPEECL biosensor displayed superior sensitivity and detection limit (Table S2).

Selectivity, Stability, Reproducibility and Real Sample Analysis of the miRNA Based SPEECL Biosensor. The selectivity of the sensing system is another important parameter for a biosensor. In order to explore the selectivity of the present SPEECL biosensor, the response towards 10 pM of miRNA-101, miRNA-155, and single-base mismatched miRNA-21 (SM miRNA-21) comparing with that of 1 fM of miRNA-21 was assayed by the present biosensor. As shown in Figure 6C, there is no obvious ECL signal towards miRNA-155, miRNA-101 or SM miRNA-21. Meanwhile, compared with miRNA-21 (1 fM), the SPEECL biosensor has no distinct difference towards its mixture containing 10 pM unspecific miRNA. The obvious higher response towards miRNA-21 implied other similar miRNA didn't interfere on miRNA-21.

Therefore, the designed SPEECL biosensor exhibited satisfying selectivity towards miRNA-21.

Stability is a vital parameter to evaluate the behaviour of the biosensor. For the purpose to judge whether the present SPEECL biosensor could satisfy the requirement of long-term cyclic use, the AgNCs/H2-H1/AuNPs/GCE in the presence of 1 fM of miRNA-21 was continuously scanned and recorded. As Figure 6D displayed, the ECL signal remained almost no obvious decay (RSD = 1.61%) after continuously scanning for 15 cycles, suggesting the favorable stability of the present SPEECL biosensor. Following that, the reproducibility of the AgNCs/H2-H1/AuNPs/GCE was tested by assaying miRNA-21 (1 fM) for 8 times repeatedly in the intra- and inter-assay. The RSD values were 3.8% and 4.6% (Figure S5), respectively, demonstrating that the acceptable reproducibility of the present miRNA-21 SPEECL biosensor.

Finally, the practical utility of the present miRNA-21 SPEECL biosensor was investigated by the assay in real samples. The samples were prepared by the spiked addition of miRNA-21 solution into 10% diluted normal human serum. As shown in Table 1, the results displayed favorable recoveries from 96% to 106% and RSDs from 3.4% to 5.3%, suggesting that the developed method is promising to determine miRNA-21 in clinical analysis.

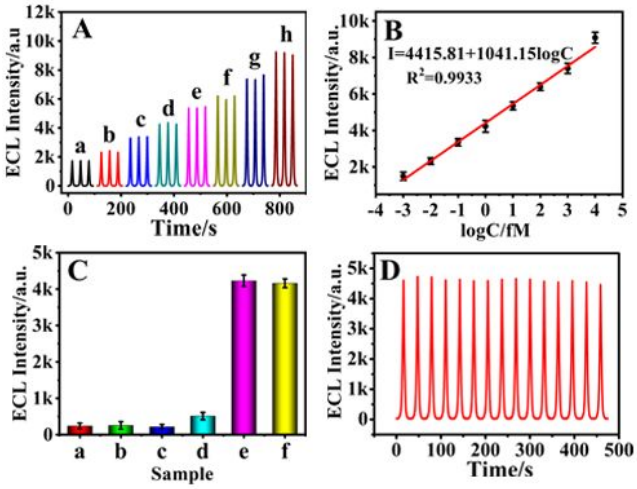

Figure 6. (A) ECL of the proposed SPEECL sensor with different concentrations of miRNA-21: (a) 10^{-3}, (b) 10^{-2}, (c) 10^{-1}, (d) 1, (e) 10, (f) 10^{2}, (g) 10^{3} and (h) 10^{4} fM. (B) Linear relationship between the ECL intensities and the logarithm of miRNA-21 concentrations. (C) ECL of the present SPEECL biosensor in blank (a) or with 10 pM miRNA-155 (b), miRNA-101 (c), SM miRNA-21 (d), 1 fM miRNA-21 (e) or their mixtures (f); (D) ECL response of AgNCs/H2-H1/AuNPs/GCE after scanned for 15 cycles continuously.

Table 1. Recovery Tests for miRNA-21 in Spiked Human Serum Samples (n = 3)

samples	added/fM	found/fM	RSD/%	recovery(%)
1	1	1.03	4.7	103
2	10	9.6	5.3	96
3	10^2	101	4.5	101
4	10^3	9700	3.6	97
5	10^4	10600	3.4	106

CONCLUSION

In summary, SPEECL with DNA templated AgNCs as ECL luminophores and the LSPR enhanced sources of AuNPs was explored and designed for the fabrication of miRNA-21 biosensor with high sensitivity and selectivity. In addition, it has demonstrated that the separation distance between AgNCs and AuNPs and the electrodeposition time of AuNPs are key to obtain optimal SPEECL. Based on the LSPR of AuNPs enhanced AgNCs ECL emission, a target miRNA-21-triggered catalyzed hairpin assembly with the enzyme-free recycling amplification strategy was developed to detect miRNA-21 with high sensitivity and selectivity, which provide a potential tool for the determination of miRNA in real applications.

ASSOCIATED CONTENT

Supporting Information

Materials and reagents; apparatus; DNA sequences; Figure S1-S5; Table S1-S2. This material is available free of charge via the Internet at http://pubs.acs.org.

AUTHOR INFORMATION

Corresponding Author

*E-mail: wangyuz@mail.ahnu.edu.cn

Notes

The authors declare no competing financial interests.

ACKNOWLEDGMENT

This work was financially supported by the National Natural Science Foundation of China (Grants 21675001), the Anhui Provincial Natural Science Foundation (1608085MB46, 1608085MC67), the Anhui Provincial Education Department Natural Sciences Key Fund (KJ2016SD23), the Key Program in the Youth Elite Support Plan in Universities of Anhui Province (gxyqZD2016023), Provincial Project of Natural Science Research for Colleges and Universities of Anhui Province of China (KJ2016A274).

REFERENCES

(1) Ding, X.; Liow, C. H.; Zhang, M.; Huang, R.; Li, C.; Shen, H.; Liu, M.; Zou, Y.; Gao, N.; Zhang, Z.; Li, Y.; Wang, Q.; Li, S.; Jiang, J. Surface plasmon resonance enhanced light absorption and photothermal therapy in the second near-infrared window. *J. Am. Chem. Soc.* **2014,** *136*, 15684-93.

(2) Jiang, R.; Li, B.; Fang, C.; Wang, J. Metal/Semiconductor hybrid nanostructures for plasmon-enhanced applications. *Adv. Mater.* **2014,** *26,* 5274-309.

(3) Klinkova, A.; Choueiri, R. M.; Kumacheva, E. Self-assembled plasmonic nanostructures. *Chem. Soc. Rev.* **2014,** *43*, 3976-91.

(4) Li, C. Y.; Meng, M.; Huang, S. C.; Li, L.; Huang, S. R.; Chen, S.; Meng, L. Y.; Panneerselvam, R.; Zhang, S. J.; Ren, B.; Yang, Z. L.; Li, J. F.; Tian, Z. Q. "Smart" Ag Nanostructures for Plasmon-Enhanced Spectroscopies. *J. Am. Chem. Soc.* **2015,** *137*, 13784-7.

(5) Visaveliya, N.; Kohler, J. M. Microfl uidic Assisted Synthesis of Multipurpose Polymer Nanoassembly Particles for Fluorescence, LSPR, and SERS Activities. *Small* **2015,** *11*, 6435-6443.

(6) Shen, Y. B.; He, T.; Wang, W. H.; Zhan, Y. L.; Hu, X.; Yuan, B. F.; Zhou, X. C. Fluorescence enhancement on silver nanoplates at the single- and sub-nanoparticle level. *Nanoscale* **2015,** *7*, 20132-20141.

(7) Khatua, S.; Paulo, P. M. R.; Yuan, H. F.; Gupta, A.; Zijlstra, P.; Orrit, M. Resonant Plasmonic Enhancement of Single-Molecule Fluorescence by Individual Gold Nanorods. *ACS Nano* **2014,** *8*, 4440-4449.

(8) He, X. X.; Wang, W. J.; Li, S. H.; Wang, Q. R.; Zheng, W. Q.; Shi, Q.; Liu, Y. L. Localized Surface Plasmon-Enhanced Electroluminescence in OLEDs by Self-Assembly Ag Nanoparticle Film. *Nanoscale Res. Lett.* **2015,** *10*, 468, DOI: 10.1186/s11671-015-1176-9.

(9) Wang, D. F.; Li, Y. Y.; Lin, Z. Y.; Qiu, B.; Guo, L. H. Surface-Enhanced Electrochemiluminescence of Ru@SiO_2 for Ultrasensitive Detection of Carcinoembryonic Antigen. *Anal. Chem.* **2015,** *87*, 5966-5972.

(10) Wang, J.; Shan, Y.; Zhao, W. W.; Xu, J. J.; Chen, H. Y. Gold Nanoparticle Enhanced Electrochemiluminescence of CdS Thin Films for Ultrasensitive Thrombin Detection. *Anal. Chem.* **2011,** *83*, 4004-4011.

(11) Zhou, H.; Han, T. Q.; Wei, Q.; Zhang, S. S. Efficient Enhancement of Electrochemiluminescence from Cadmium Sulfide Quantum Dots by Glucose Oxidase Mimicking Gold Nanoparticles for Highly Sensitive Assay of Methyltransferase Activity. *Anal. Chem.* **2016,** *88*, 2976-2983.

(12) Li, M. X.; Zhang, N.; Zhao, W.; Luo, X. L.; Chen, H. Y.; Xu, J. J. Ultrasensitive detection of microRNA-21 based on plasmon-coupling-induced electrochemiluminescence enhancement. *Electrochem. Commun.* **2018,** *94*, 36-40.

(13) Gong, T. C.; Zhang, J.; Zhu, Y.; Wang, X. Y.; Zhang, X. L.; Zhang, J. Optical properties and surface-enhanced Raman scattering of hybrid structures with Ag nanoparticles and graphene. *Carbon* **2016,** *102*, 245-254.

(14) Mezni, A.; Dammak, T.; Fkiri, A.; Mayah, A.; Abid, Y.; Smiri, L. S. Photochemistry at the Surface of Gold Nanoprisms from Surface-Enhanced Raman Scattering Blinking. *J. Phys. Chem. C.* **2014,** *118*, 17956-17967.

(15) Matthews, J. R.; Payne, C. M.; Hafner, J. H. Analysis of Phospholipid Bilayers on Gold Nanorods by Plasmon Resonance Sensing and Surface-Enhanced Raman Scattering. *Langmuir* **2015,** *31*, 9893-9900.

(16) Brown, L. V.; Zhao, K.; King, N.; Sobhani, H. Nordlander, P.; Halas, N. J. Surface-Enhanced Infrared Absorption Using Individual Cross Antennas Tailored to Chemical Moieties. *J. Am. Chem. Soc.* **2013,** *135*, 3688-3695.

(17) Strekal, N.; Maskevich, A.; Maskevich, S.; Jardillier, J. C.; Nabiev, I. Selective enhancement of Raman or fluorescence spectra of biomolecules using specifically annealed thick gold films. *Biopolymers* **2000,** *57*, 325-328.

(18) Jung, J. M.; Yoo, H. W.; Stellacci, F.; Jung, H. T. Two-Photon Excited Fluorescence Enhancement for Ultrasensitive DNA Detection on Large-Area Gold Nanopatterns. *Adv. Mater.* **2010,** *22*, 2542-2546.

(19) Wang, D.; Guo, L.; Huang, R.; Qiu, B.; Lin, Z.; Chen, G. Surface enhanced electrochemiluminescence of $Ru(bpy)_3^{2+}$. *Sci. Rep.* **2015**, *5*, 7954, DOI: 10.1038/srep07954.

(20) Li, R.; Yan, R.; Bao, J.; Tu, W.; Dai, Z. A localized surface plasmon resonance-enhanced photoelectrochemical biosensing strategy for highly sensitive and scatheless cell assay under red light excitation. *Chem. Commun.* **2016,** *52*, 11799-11802.

(21) Zhang, J.; Gryczynski, Z.; Lakowicz, J. R. First observation of surface plasmon-coupled electrochemiluminescence. *Chem. Phys. Lett.* **2004,** *393*, 483-487.

(22) Chowdhury, M. H.; Malyn, S. N.; Aslan, K.; Lakowicz, J. R.; Geddes, C. D. First observation of surface plasmon-coupled chemiluminescence (SPCC). *Chem. Phys. Lett.* **2007,** *435*, 114-118.

(23) Shan, Y.; Xu, J. J.; Chen, H. Y. Distance-dependent quenching and enhancing of electrochemiluminescence from a CdS:Mn nanocrystal film by Au nanoparticles for highly sensitive detection of DNA. *Chem. Commun.* **2009**, *8*, 905-7.

(24) Huo, X. L.; Zhang, N.; Yang, H.; Xu, J. J.; Chen, H. Y. Electrochemiluminescence Resonance Energy Transfer System for Dual-Wavelength Ratiometric miRNA Detection. *Anal. Chem.* **2018,** *90*, 13723-13728.

(25) Zhang, W.; Xiong, H. W.; Chen, M. M.; Zhang, X. H.; Wang, S. F. Surface-enhanced molecularly imprinted electrochemiluminescence sensor based on Ru@SiO_2 for ultrasensitive detection of fumonisin B_1. *Biosens. Bioelectron.* **2017,** *96*, 55-61.

(26) Deng, L.; Du, Y.; Xu, J. J.; Chen, H. Y. An off-on-off electrochemiluminescence approach for ultrasensitive detection of thrombin. *Biosens. Bioelectron.* **2014,** *59*, 58-63.

(27) Liu, Y.; Chen, X. Q.; Ma, Q. A novel amplified electrochemiluminescence biosensor based on Au NPs@PDA@CuInZnS QDs nanocomposites for ultrasensitive detection of p53 gene. *Biosens. Bioelectron.* **2018,** *117*, 240-245.

(28) Li, X.; Xu, Y.; Chen, Y.; Wang, C.; Jiang, J.; Dong, J.; Yan, H.; Du, X. Dual Enhanced Electrochemiluminescence of Aminated Au@SiO_2/CdS Quantum Dot Superstructures: Electromagnetic Field Enhancement and Chemical Enhancement. *ACS Appl. Mater. Interfaces.* **2019,** *11*, 4488-4499.

(29) Javani, S.; Lorca, R.; Latorre, A.; Flors, C.; Cortajarena, A. L.; Somoza, A. Antibacterial Activity of DNA-Stabilized Silver Nanoclusters Tuned by Oligonucleotide Sequence. *ACS Appl. Mater. Interfaces* **2016,** *8*, 10147-10154.

(30) Jie, G. F.; Tan, L.; Zhao, Y.; Wang, X. C. A novel silver nanocluster in situ synthesized as versatile probe for electrochemiluminescence and electrochemical detection of thrombin by multiple signal amplification strategy. *Biosens. Bioelectron.* **2017,** *94*, 243-249.

(31) Zhang, L. B.; Zhu, J. B.; Zhou, Z. X.; Guo, S. J.; Li, J.; Dong, S. J. Wang, E. K. A new approach to light up DNA/Ag nanocluster-based beacons for bioanalysis. *Chem. Sci.* **2013,** *4*, 4004-4010.

(32) Li, J. J.; Wang, W. J.; Sun, D. F.; Chen, J. N.; Zhang, P. H. Zhang, J. R.; Min, Q. H.; Zhu, J. J. Aptamer-functionalized silver nanoclusters-mediated cell type-specific siRNA delivery and tracking. *Chem. Sci.* **2013,** *4*, 3514-3521.

(33) Del Bonis-O'Donnell, J. T.; Vong, D.; Pennathur, S.; Fygenson, D. K. A universal design for a DNA probe providing ratiometric fluorescence detection by generation of silver nanoclusters. *Nanoscale* **2016,** *8*, 14489-14496.

(34) Zhang, L. B.; Zhu, J. B.; Guo, S. J.; Li, T.; Li, J.; Wang, E. K. Photoinduced Electron Transfer of DNA/Ag Nanoclusters Modulated by G-Quadruplex/Hemin Complex for the Construction of Versatile Biosensors. *J. Am. Chem. Soc.* **2013,** *135*, 2403-2406.

(35) Yin, J. J.; He, X. X.; Wang, K. M.; Qing, Z. H.; Wu, X.; Shi, H. Yang, X. H. One-step engineering of silver nanoclusters-aptamer assemblies as luminescent labels to target tumor cells. *Nanoscale* **2012,** *4*, 110-112.

(36) Diez, I.; Pusa, M.; Kulmala, S.; Jiang, H.; Walther, A. Goldmann, A. S.; Muller, A. H. E.; Ikkala, O.; Ras, R. H. A. Color Tunability and Electrochemiluminescence of Silver Nanoclusters. *Angew. Chem., Int. Ed.* **2009,** *48*, 2122-2125.

(37) Tao, Y.; Ran, X.; Ren, J. S.; Qu, X. G. Array-Based Sensing of Proteins and Bacteria By Using Multiple Luminescent Nanodots as Fluorescent Probes. *Small* **2014,** *10*, 3667-3671.

(38) Zhou, Y.; Chen, M. X.; Zhuo, Y.; Chai, Y. Q.; Xu, W. J.; Yuan, R. In Situ Electrodeposited Synthesis of Electrochemiluminescent Ag Nanoclusters as Signal Probe for Ultrasensitive Detection of Cyclin-D1 from Cancer Cells. *Anal. Chem.* **2017,** *89*, 6787-6793.

(39) Zhou, Y.; Wang, H. J.; Zhuo, Y.; Chai, Y. Q.; Yuan, R. Highly Efficient Electrochemiluminescent Silver Nanoclusters/Titanium Oxide Nanomaterials as a Signal Probe for Ferrocene-Driven Light Switch Bioanalysis. *Anal. Chem.* **2017,** *89*, 3732-3738.

(40) Chen, A. Y.; Ma, S. Y.; Zhuo, Y.; Chai, Y. Q.; Yuan, R. In Situ Electrochemical Generation of Electrochemiluminescent Silver Naonoclusters on Target-Cycling Synchronized Rolling Circle Amplification Platform for MicroRNA Detection. *Anal. Chem.* **2016,** *88*, 3203-3210.

(41) Zhang, Y. Y.; Feng, Q. M.; Xu, J. J.; Chen, H. Y. Silver Nanoclusters for High-Efficiency Quenching of CdS Nanocrystal Electrochemiluminescence and Sensitive Detection of microRNA. *ACS Appl. Mater. Interfaces* **2015,** *7*, 26307-26314.

(42) Li, M. X.; Zhao, W.; Qian, G. S.; Feng, Q. M.; Xu, J. J.; Chen, H. Y. Distance mediated electrochemiluminescence enhancement of CdS thin films induced by the plasmon coupling of gold nanoparticle dimers. *Chem. Commun.* **2016,** *52*, 14230-14233.

(43) Neumann, T.; Johansson, M. L.; Kambhampati, D.; Knoll, W. Surface-plasmon fluorescence spectroscopy. *Adv. Funct. Mater.* **2002,** *12*, 575-586.

(44) Kulakovich, O.; Strekal, N.; Yaroshevich, A.; Maskevich, S.; Gaponenko, S.; Nabiev, I.; Woggon, U.; Artemyev, M. Enhanced luminescence of CdSe quantum dots on gold colloids. *Nano Lett.* **2002,** *2*, 1449-1452.

(45) Tabakman, S. M.; Lau, L.; Robinson, J. T.; Price, J.; Sherlock, S. P.; Wang, H.; Zhang, B.; Chen, Z.; Tangsombatvisit, S.; Jarrell, J. A.; Utz, P. J.; Dai, H. Plasmonic substrates for multiplexed protein microarrays with femtomolar sensitivity and broad dynamic range. *Nat. Commun.* **2011,** *2*, 466, DOI: 10.1038/ncomms1477.

Table of Contents graphic: